# Polymer Chemistry

Accepted Manuscript






ROYAL SOCIETY OF CHEMISTRY

www.rsc.org/polymers

Journal Name

ARTICLE

# Effect of Chain Curvature on the Performance of Diketopyrrolopyrrole-Based Polymer Solar Cells

Received 00th January 20xx,
Accepted 00th January 20xx

DOI: 10.1039/x0xx00000x

www.rsc.org/

Hui Li,[a, b] Xiaolin Zheng,[c] Xuedong Wang,[a, b] Fangbin Liu,[a, b] and Hongbing Fu*[a, c]

Two novel polymers, **PDTBO** and **PD2TBO**, containing diketopyrrolopyrrole and alkoxyl-substituted benzothiadiazole were designed and synthesized for polymer photovoltaics. Introduction of thiophene and bithiophene as different π-bridge units results in good planarity of polymer backbone but different curvature in polymer chains. Inclusion of bithiophene in repeat unit leads to a potentially larger curvature and a zigzag conformation for **PD2TBO**. This increased curvature does not damage the thin-film crystallinity. Instead, high hole mobility is recorded for **PD2TBO** which is almost two orders of magnitude higher than that of linear **PDTBO**. Furthermore, high power conversion efficiency (PCE) of 5.3% is obtained for **PD2TBO**/$PC_{71}BM$ blend film ascribed to good miscibility while the linear polymer **PDTBO** exhibits a moderate PCE of 2.1%. Our work demonstrates that the modulation of chain curvature is an efficient approach to improve the performance of polymer solar cells.

## Introduction

Considerable progress has been made in the improving the performance of polymer solar cells in recent years.[1-3] The power conversion efficiency (PCE) of bulk-heterojunction solar cells containing conjugated polymers as donor and fullerene as acceptor has reached up to 8-9%.[3,4] Extensive efforts have been focused on designing and synthesizing new polymers to broaden the absorption range,[5,6] tune their energy levels[7] and improve phase separation.[8-10] The general strategy is the alternative copolymerization of proper electron-rich (D) unit and electron-deficient (A) unit in the polymer chain as D-A type polymer.[11,12] Among the various conjugated units, diketopyrrolopyrrole (DPP) has attracted tremendous attention and exhibited high performance in thin-film devices.[13-16] Low conformational disorder and highly coplanar skeleton of DPP promote a more delocalized orbital distribution along the backbone and strong π-π stacking, which enhance intramolecular and intermolecular charge-carrier hopping.[17] Systematical research on molecular weight,[18,19] side chain engineering,[13,20,21] and aggregation behavior[22] have shed light on the relationship between structure and properties of DPP-based polymers and small molecules. However, curvature, as a crucial aspect for polymer chain spatial geometry, however, is paid little attention to DPP-based polymer semiconductors. In the past, the curving of π-conjugated polymers was mostly induced by the nonlinear monomer geometry.[23,24,25] Klaus Müllen group investigated a series of polymers in which different degree of curvature of benzodithiophene isomers influence solubility, energy levels, and film morphology. As a result, intermediate degree of curvature yielded the highest charge-carrier mobilities. Recently, Woo group presented that "conformational locking" in polymer backbone induced the curvature of chains and dramatically influenced the PCE of solar cells.[26,27] Therefore, the modulation of polymer curvature via rational molecular design seems to be a new strategy to improve the performance of polymer photovoltaics.

To better understand how the curvature of polymer chain determines the solid-state structure and governs the intrinsic optoelectronic properties of DPP-based polymers, we synthesized **PDTBO** and **PD2TBO**, containing DPP and alkoxyl-substituted benzothiadiazole (BTDO) as building blocks, with the different thiophene number in polymer backbone as π-bridge units. With one thiophene incorporating into polymer chain, **PDTBO** shows linear conformation while bithiophene incorporated between DPP and BTDO in polymer backbone induces a zigzag conformation in **PD2TBO**. Two-dimensional grazing incidence X-ray diffraction indicates the increased curvature does not damage the thin-film crystallinity, instead, high hole mobility is recorded for **PD2TBO** which is almost two orders of magnitude higher than that of **PDTBO**. Furthermore, high power conversion efficiency of 5.3% was achieved for **PD2TBO**/$PC_{71}BM$ blend film attributing good miscibility while a moderate PCE of 2.1% was obtained for device based on **PDTBO**/$PC_{71}BM$ blend film.

[a] *Beijing National Laboratory for Molecular Sciences, Institute of Chemistry, Chinese Academy of Sciences, Beijing 100190, P. R. China. Email: hongbing.fu@iccas.ac.cn*
[b] *University of Chinese Academy of Sciences, Beijing 100049, P. R. China*
[c] *Beijing Key Laboratory for Optical Materials and Photonic Devices, Department of Chemistry, Capital Normal University, Beijing 100048, P. R. China*
† Electronic Supplementary Information (ESI) available: GPC results, TGA and DSC measurements, film absorption, DFT calculation, OFET properties, blend film absorption and AFM images. See DOI: 10.1039/x0xx00000x

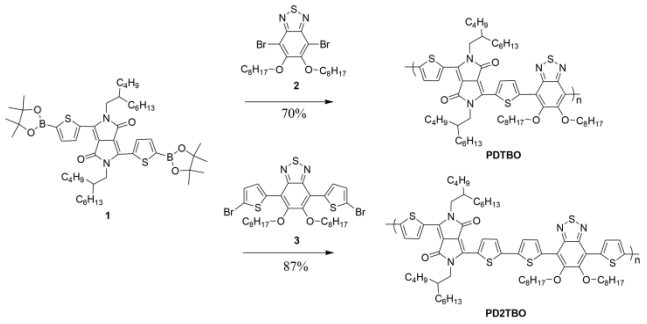


**Scheme 1** Synthetic Route of Polymer **PDTBO** and **PD2TBO**

## Results and discussion

### Material synthesis and characterization

The synthetic routes to two polymers are shown in Scheme 1. Monomer **1** was synthesized from the reaction of thienyl-substituted diketopyrrolopyrrole with lithium diisopropylamide and quenching with isopropoxyboronic acid pinacol ester.[28] The resulting monomer was purified via recrystallization using methanol carefully. Monomer **2** was commercially available and monomer **3** was synthesized according to literature work.[29] The typical palladium-catalyzed Suzuki coupling in toluene was used to obtain polymers. In order to exclude the influence of molecular weight, careful control of polymerization condition was realized. Very close number-average molecular weights (17.7 kDa and 18.3 kDa for **PDTBO** and **PD2TBO**, respectively) and polydispersity (PDI) (2.2 and 2.7 for **PDTBO** and **PD2TBO**, respectively) were obtained for two polymers by carrying out high temperature gel permeation chromatography (GPC) at 150 °C with 1,2,4-trichlorobenzene as the eluent, as shown in Table 1 and Fig. S1 †. Two polymers show good thermal stability with deposition temperatures ($T_d$) over 320 °C (Fig. S2†). Employing differential scanning calorimetry (DSC), only **PDTBO** exhibits an endothermic peak at 269 °C while there is no thermal transition is observed for **PD2TBO** (Fig. S3†).

### Photophysical and electrochemical properties

We record the UV-vis absorption spectra of two polymers in dilute chloroform solution and thin film (Fig. 1a). To our surprise, even though the longer repeat unit is existent, **PD2TBO** exhibits obviously hypochromic shift absorption with difference of ~ 100 nm compared with **PDTBO** at maximum absorption wavelength both in the solution and in solid state.

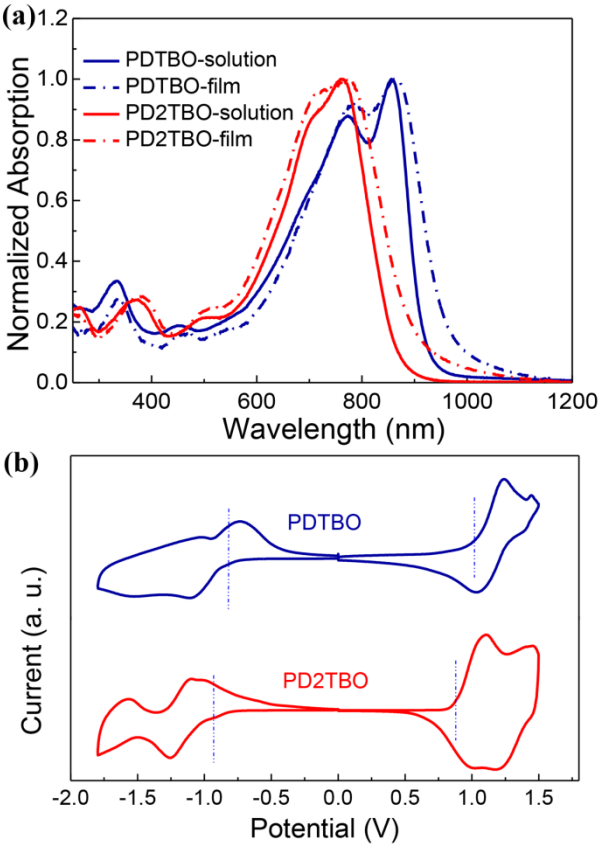


**Fig. 1** (a) Normalized absorption spectra of **PDTBO** and **PD2TBO** in $CHCl_3$ solution (solid line) and in solid state films (dash dot line). (b) Cyclic voltammograms of two polymer thin films.

This result is contrary to the general expectation that increasing the number of thiophene unit contributes to the conjugated length.[30,31] Therefore, we believe that the polymer chains of **PD2TBO** constitute special conformation which somewhat disrupts the "push-pull" effect between donor and acceptor moieties and reduces the efficient conjugation length. Both polymers display strong low energy bands absorption (600 nm ~ 950 nm) attributed to intrachain charge transfer (ICT).[32] Going from solution to film state, significantly bathochromic shifts (~ 30 nm) in absorption onset were observed and the shoulder peaks become intense for two polymers, which could be attributed to solid-state packing effects.[33] After annealed at 150 °C for 30 min, the intensities of the shorter-wavelength shoulders of two polymer films further increase although the absorption range do not show significant

**Table 1** Molecular weights, thermostability, optical and electrochemical properties of two polymers

| polymer | $M_n$ (KDa) | PDI | $T_d$ °C | $T_g$ °C | $\lambda_{max}$ (nm) solution | $\lambda_{max}$ (nm) film | HOMO (eV)[a] | LUMO (eV)[a] | $E_g^{opt}$ (eV)[b] | $E_g^{CV}$ (eV)[c] |
|---|---|---|---|---|---|---|---|---|---|---|
| PDTBO | 17.7 | 2.2 | 320 | 269 | 774, 856 | 782, 863 | -5.36 | -3.84 | 1.30 | 1.52 |
| PD2TBO | 18.3 | 2.7 | 329 | — | 709, 760 | 719, 770 | -5.18 | -3.60 | 1.38 | 1.58 |

[a]Cyclic voltammetry determined with $Fc/Fc^+$ ($E_{HOMO}$ = - 4.80 eV) as external reference. [b]Band gaps were calculated from the onset of the film absorption. [c]$E_g^{CV} = E_{LUMO}$-$E_{HOMO}$

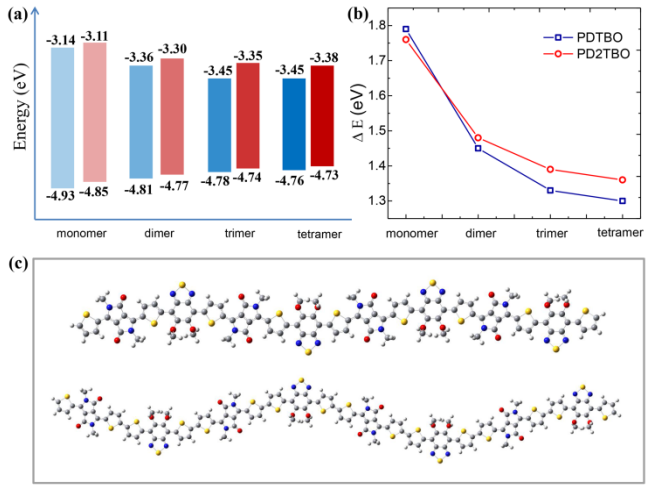


**Fig. 2** (a) Calculated orbital energy levels of monomer, dimer, trimer, and tetramer for **PDTBO** (blue bar) and **PD2TBO** (red bar) using DFT (B3LYP/6-31G). (b) Calculated band gaps of monomer, dimer, trimer, and tetramer for two polymers ($\Delta E = E_{LUMO}$-$E_{HOMO}$). (c) The minimum-energy conformations of tetramers for two polymers.

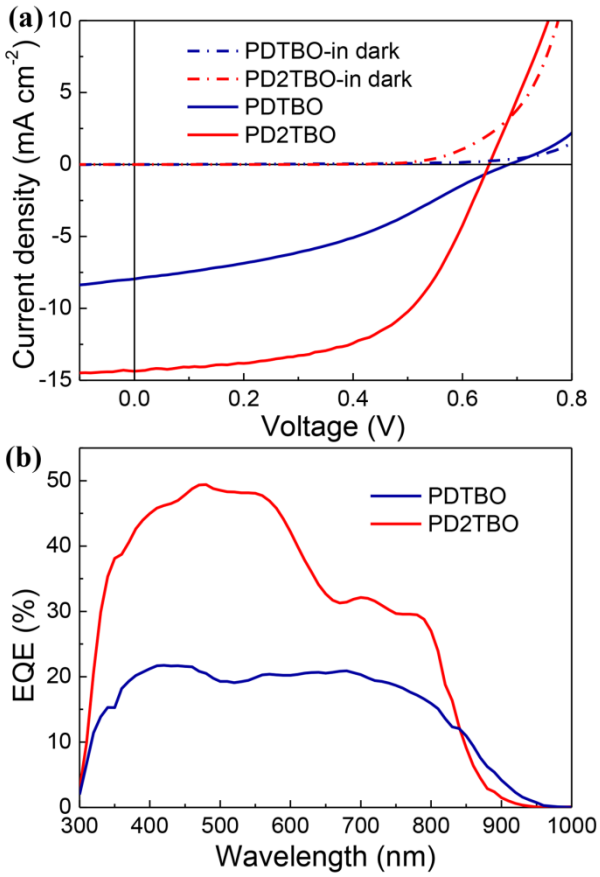


**Fig. 3** (a) *J-V* characteristics in dark (dash dot lines) and under white light illumination (solid lines) of the optimized solar cells based on polymer/$PC_{71}BM$. (b) EQE spectra of the optimized devices based on two polymers.

difference (Fig. S4†). By employing cyclic voltammetry (CV) measurements on thin films, the lowest unoccupied molecular orbit (LUMO)/the highest occupied molecular orbit (HOMO) extracted from the onset of the reduction waves and oxidation waves[8] are displayed in Fig. 1b and summarized in Table 1. The LUMO/HOMO energy levels for **PDTBO** are -3.84/-5.36 eV. For **PD2TBO**, the LUMO/HOMO energy levels are -3.60/-5.18 eV. The incorporation of one more thiophene raises the LUMO and HOMO energy levels, simultaneously, attributing to the electro-rich character of thiophene. The larger electrochemical band gap of **PD2TBO** than that of **PDTBO** is in accordance with the result of optical measurement.

### DFT calculations

To investigate how the chain geometry induces the high-energy absorption of **PD2TBO**, we simulated the orbital energy levels of two polymers by changing the number of repeat units (Fig. 2a). Before that, it is requisite to optimize the geometries of two building blocks, thienyl-substituted DPP and thienyl-substituted BTDO. The alkyl chains were replaced with methyl groups for computational simplicity. For thienyl-substituted DPP, the present of intramolecular hydrogen bonds arising from the protruding carbonyl group and neighboring thiophene units ensures the planar backbone and the minimum-energy conformation.[34] By changing the torsional angle between thiophene and BTDO moieties, the optimized conformation was calculated to be the structure III (Fig. S5†) in which C-H…N and S…O non-covalent inter-actions allow for a planar structure. According to these results, increasing the repeat units, we found that the band gaps of two polymers decrease simultaneously. For monomers of two polymers, **PD2TBO** exhibits smaller band gap than that of **PDTBO** because of its longer π-conjugated backbone. However, this phenomenon is broken in dimers. As shown in Fig. 2b, in dimer, trimer and tetramer, the band gaps of **PD2TBO** are significant larger than those of **PDTBO**. It is noteworthy that all these oligomers possess good planarity even for the tetramers (Fig. S6†), which excludes the influence of distortion of backbone on the effective conjugation length. From the minimum energy conformation of these oligomers, it can be obviously observed that the dramatic difference between two polymers is the chain curvature (Fig. S7†). For **PDTBO**, the chain remains linear pattern with the increase of repeat unit while the chain of **PD2TBO** trends to form a zigzag conformation from the dimer and the chain curvature is apparent in tetramer (Fig. 2c). Therefore, the curved conformation reduces the effective conjugation length of backbone and results in blue-shift absorption of **PD2TBO**.

### Photovoltaic device performance

Solution-processed photovoltaic devices were fabricated using a conventional device structure of ITO/PEDOT:PSS/polymer:$PC_{71}BM$/Ca/Al. The performance of devices were carefully optimized by varying the layer thickness, the spin-coating solvent, the weight ratio of donor and acceptor, the temperature of post-treatment, etc. With a series of testing, the ratio of polymer to $PC_{71}BM$ was kept at 1:3 in this work. 1, 8-Diiodooctane (DIO) was used as an additive with the concentration of 1% volume in chlorobenzene. Fig. 3a shows the corresponding current density versus voltage (*J-V*) characteristics of two optimal devices. Table 2 and Table S1 summarized the photovoltaic

**Table 2** Characteristic properties of bulk heterojunction solar cells based on 1:3 weight ratio of polymer and $PC_{71}BM$ for **PDTBO** and **PD2TBO**, respectively

| polymer | Annealing °C | $V_{oc}$ (V) | $J_{sc}$ (mA $cm^{-2}$) | FF (%) | PCE[a] (%) |
|---|---|---|---|---|---|
| PDTBO | 120 | 0.69 | 7.6 | 0.41 | 2.1 (2.0±0.005) |
| PD2TBO | 110 | 0.65 | 14.4 | 0.56 | 5.3 (5.2±0.006) |

[a]The average values collected more than 8 devices are shown in parenthesis

parameters for these devices. For **PD2TBO** devices, a remarkable short-circuit current density ($J_{sc}$) of 14.4 mA $cm^{-2}$ in combination with a high fill factor (FF) of 0.56 gave a PCE of 5.3%. The PDTBO/$PC_{71}BM$ devices gave a moderate PCE of 2.1% with decreased $J_{sc}$ of 7.6 mA $cm^{-2}$ and FF of 0.41. Open-circuit voltage ($V_{oc}$) (0.65 V) of **PD2TBO** devices is smaller than that of **PDTBO** devices (0.69 V) which accords with the fact that $V_{oc}$ is mainly determined by the difference between the HOMO energy levels of donor materials and LUMO energy level of $PC_{71}BM$.[35] For optimized devices, the EQE spectra agree well with the $J_{sc}$ obtained from *J-V* measurement (Fig. 3b). The $J_{sc}$ integrated from EQE data are 7.2 mA $cm^{-2}$ and 13.7 mA $cm^{-2}$ for **PDTBO** and **PD2TBO**, respectively (within 5% error). It indicates that the exciton generation is more efficient in **PD2TBO**-based devices than that of **PDTBO**-based device.[36]

### Thin film morphology and microstructural analysis

We investigate the microstructure of pure polymer films and blend films via two-dimensional grazing incidence X-ray diffraction (2D-GIXRD) to illustrate how the chain curvature influences the morphology and the performance of thin-film devices. Two pure polymers exhibit different orientations in thin films. In Fig. 4a, in the out of plane, **PDTBO** displays strong diffraction peak at 2θ = 5.0° and 2θ = 24° corresponding to lamellar distance of 17.7 Å and π-π stacking distance of 3.7 Å, respectively. In addition, the lamellar structures can also be observed in the in-plane pattern indicating there is no preferential orientation formed in **PDTBO** film. In contrast, for **PD2TBO** thin film (Fig. 4b), in the out of plane pattern, clear diffraction signals at 2θ = 5.1° with the second diffraction peak corresponding to lamellar distance of 17.4 Å, meanwhile, π-π stacking diffraction at 2θ = 24° corresponding to *d*-spacing of 3.7 Å exists in plane pattern. This indicates that the polymer chains prefer to constitute edge-on orientation and the curvature of backbone has no impact on π-π stacking distance. The slightly shorter lamellar distance and the preferential orientation of **PD2TBO** indicate that alkyl chains intercalate each other more intensely and much ordered stacking exists in the thin film. Topographical information of annealed polymer films obtained from atomic force microscopy (AFM) indicates that **PD2TBO** film exhibits more intense packing with larger $R_a$ (average roughness) than that of **PDTBO** film (Fig. S8†), suggesting better carrier transport in **PD2TBO** film. The measurements of hole mobilities of two pure polymers confirm the results (Fig. S9†). **PD2TBO** shows good hole mobility with the highest value of 0.4 $cm^2$ $V^{-1}$ $s^{-1}$ while **PDTBO** has significantly lower mobility of 0.01 $cm^2$ $V^{-1}$ $s^{-1}$ under ambient condition (Table S2). After mixed with fullerenes, the

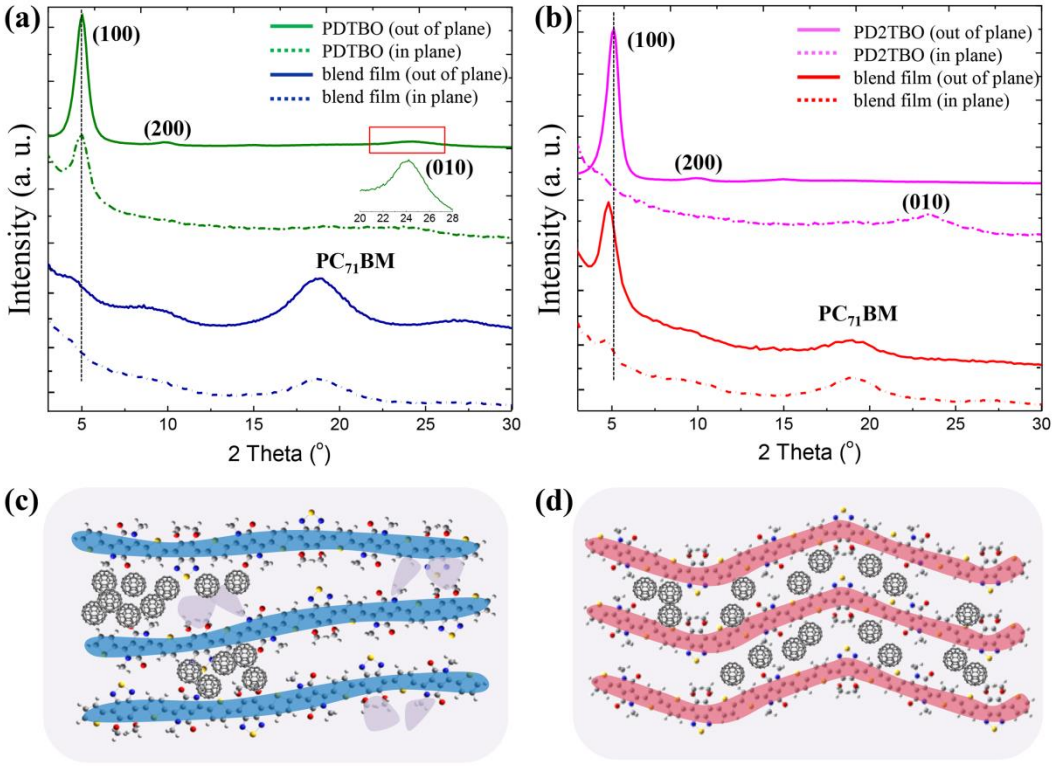


**Fig. 4** 2D-GIXRD pattern of pure polymer film and polymer/$PC_{71}BM$ blend film based on **PDTBO** (a) and **PD2TBO** (b), respectively. The schematic illustration of microstructures of **PDTBO**/$PC_{71}BM$ (c) and **PD2TBO**/$PC_{71}BM$ blend films (d), respectively. The light gray shadow in figure (c) represents steric hindrance of alkyl chains.

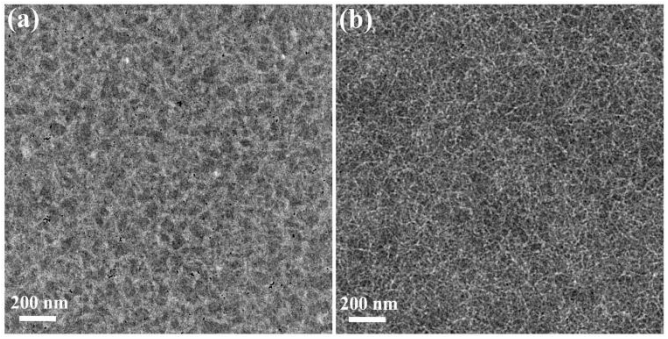


**Fig. 5** Bright field TEM images of the optimized **PDTBO**/$PC_{71}BM$ blend film (a) and **PD2TBO**/$PC_{71}BM$ blend film (b).

lamellar structures of PDTBO film are vanished both in two dimensions and strong diffraction peaks of $PC_{71}BM$ appear, which suggests that the packing of polymers are completely disturbed by fullerenes. Different from PDTBO, the PD2TBO/$PC_{71}BM$ film remains lamellar packing patterns in two dimensions. Moreover, the lamellar distance in the out of plane pattern increases to 20.7 Å. These results suggest that $PC_{71}BM$ could intercalate well into the lamellar structure of polymer chains.[37]

On the basis of above observation, the difference in crystallinity, especially the lamellar structure, between two polymers in both the pure film and blend film is markedly large and thus dramatically influences the solar cell performance. The zigzag conformation of the backbone is more favorable to form ordered and intense interlamellar packing than the straightly linear conformation. It can be attributed to bithiophene in **PD2TBO** providing enough space for adjacent alkyl chains to extend and interlock each other intensely, which to some extent reduces displacement between adjacent zigzag chains. In contrast, the reduced distance between the solubilizing alkyl chains in **PDTBO** results in increased steric interaction that could impair the polymer packing. In blend film, as illustrated in Fig. 4c, fullerenes interrupt the packing of **PDTBO** and trend to self-aggregate inducing large domains to decrease performance. However, in **PD2TBO**-based blend film, the perturbation of fullerene is relatively weak because fullerenes could intercalate well into the lamellar structures of polymers (Fig. 4d). Good miscibility is responsible for the improved photovoltaic performance. The blend film absorption spectra reveal that, compared with the featureless absorption profile of **PDTBO**-based film (Fig. S10†), the fine vibration absorption at 700 nm ~ 800 nm in **PD2TBO**-based film still exists after mixing with $PC_{71}BM$. This confirms that polymer **PD2TBO** remains its packing pattern in blend film. Transmission electron microscopy (TEM) and atomic force microscopy (AFM) were used to further probe the morphology of the blend films (Fig. 5 and Fig. S11†). As mentioned above, in **PDTBO**/$PC_{71}BM$ blend film, polymer-rich and $PC_{71}BM$-rich domains occur on a scale of 50 nm ~ 100 nm which are considered too large and thus unfavorable for exciton dissociation. On the contrary, well-defined interpenetrating networks with fibril width of ~ 20 nm are beneficial for exciton dissociation and charge transport in **PD2TBO**-based blend film.[38] From the AFM images, **PD2TBO**/$PC_{71}BM$ blend film showed smaller phase separation (~ 20 nm) domains with greater surface roughness than that of **PDTBO**/$PC_{71}BM$ blend film, suggesting its more favorable morphology for photovoltaic performance.

## Conclusions

In conclusion, two novel polymers, named **PDTBO** and **PD2TBO** were designed and synthesized. With different π-bridge, thiophene and bithiophene, similar planarity but different backbone conformation is correlated with the film crystallinity, morphology, and photovoltaic properties of **PDTBO** and **PD2TBO**. The backbone of **PDTBO** exhibits a linear backbone while **PD2TBO** has a much curved conformation. Despite zigzag structure existing, ordered interchain packing can still be formed in the film of **PD2TBO** which is responsible for high mobility of 0.4 $cm^2\ V^{-1}\ s^{-1}$ in OFET. As active layer, **PD2TBO**/$PC_{71}BM$ shows high PCE of 5.3% while **PDTBO**/$PC_{71}BM$ shows a moderate PCE of 2.1%. It suggests that the modulation of polymer chain curvature would be a useful tool to improve photovoltaic properties.

## Experimental section

### Materials and characterization

Unless otherwise specified, the starting chemical materials were purchased from Alfa and Sigma and were used without further purification. The solvents were obtained from Beijing Chemical Plant. Toluene was freshly dried over sodium and benzophenone under inert argon atmosphere. The gel permeation chromatography (GPC) measurements were performed on a Polymer Labs PL 220 system with a refractive index detector, using 1, 2, 4-trichlorobenzene (TCB) as eluent at 150 $^oC$ and polystyrene standards as calibrants. Thermogravimetric analysis (TGA) measurements were recorded by Shimadzu thermogravimetric analyzer (model DTG-60) under a dry nitrogen gas flow at a heating rate of 10 $^oC\ min^{-1}$. Differential scanning calorimetry (DSC) analysis was performed on a METTLER TOLEDO Instrument with DSC822 calorimeter. UV-vis absorption spectra were measured on a Shimidazu UV-3600 UV-VIS-NIR spectrophotometer. Elemental analyses were performed on a Flash EA 1112 elemental analyser. The electrochemical properties were characterized in a conventional three-electrode cell consisting of a platinum working electrode coated with a thin film layer of polymer, a platinum wire auxiliary electrode, and an Ag/AgCl reference electrode with ferrocenium-ferrocene ($Fc^+$-Fc) as the external standard. Tetrabutylammoniumhex-afluorophosphate ($TBAPF_6$) (0.1 M) was used as the supporting electrolyte. Atom force microscopy (AFM) was determined by Bruker Multimode 8 using tapping mode with a scan speed of 1 Hz. Transmission electron microscopy (TEM) was performed on a JEM-2011 operated at 100 kV. Grazing incidence X-ray diffraction (GIXRD) data were obtained at 1W1A, Beijing Synchrotron Radiation Facility. The films were illuminated at a constant incidence angle of 0.2° ($\lambda = 2d\sin\theta = 1.5464$ Å).

### Synthesis of PDTBO

In a Schlenk tube, 1 mL $H_2O$ solution of $K_3PO_4$ (424 mg, 2 mmol) and a drop of Aliquat 336 was added to a degassed 6 mL toluene solution of 2,5-bis(2-butyloctyl)-3,6-bis[5-(4,4,5,5-tetramethyl-1,3,2-dioxoborolan-2-yl)thiophene-2-yl]-2,5-dihydropyrrolo[3,4-c]pyrrole-1,4-dione (1) (150 mg, 0.169 mmol) and 4,7-dibromo-5,6-bis(octyloxy)-benzothiadiazole (2) (93 mg, 0.169 mmol). The solution degassed before $Pd_2(dba)_3$ (4.6 mg, 0.005 mmol) and P(*o*-tol)$_3$ (6.2 mg, 0.02 mmol) were added. After heated to 120 $^oC$ for 48 h, the mixture was cooled to room temperature and poured into a mixture of methanol and water. The resulting precipitate was purified by Soxhlet extraction successively with methanol, acetone, hexane, and finally with chloroform, and then precipitated in methanol again. The polymer PDTBO was obtained as purple solids (167 mg, 70%). Anal. Calcd for $C_{60}H_{90}N_4O_4S_3$: C, 70.13; H, 8.83; N, 5.45. Found: C, 69.95; H, 8.80; N, 5.29%.

### Synthesis of PD2TBO

To ensure the similar molecular weight, the synthetic procedures of PD2TBO were almost the same as that of PDTBO. The polymer PDTBO was obtained as purple solids (152 mg, 87%) Anal. Calcd for $C_{68}H_{94}N_4O_4S_5$: C, 68.53; H, 7.95; N, 4.70. Found: C, 68.31; H, 7.63; N, 4.65%.

### OFET device preparation and characterization

The OFET devices were prepared with bottom-gate/top-contact configuration. The $SiO_2$/Si substrates were cleaned and treated with octadecyltrichlorosilane (OTS). Polymer solution in chlorobenzene (4 mg mL$^{-1}$) was spin coated at a speed of 2000 rpm for 50 s. The samples were thermal annealed at 150 $^oC$ in $N_2$ for 30 min. Then gold source and drain electrodes (60 nm) were deposited by vacuum evaporation on the organic layer through a shadow mask. The channel length ($L$) and width ($W$) were 30 μm and 500 μm, respectively. Field-effect mobilities were determined at room temperature in air by using a Keithley 4200 SCS. The mobility in the saturation region was extracted from the following equation:

$I_{DS}=C_i\mu(W/2L)(V_G-V_T)^2$

where $I_{DS}$ is the drain current, $C_i$ is the capacitance of the $SiO_2$ dielectric layer ($C_i$ = 10 nF cm$^{-2}$), $\mu$ is the mobility, $V_G$ and $V_T$ are the gate voltage and threshold voltage, respectively.

### OPV devices fabrication and testing

The photovoltaic devices were fabricated with conventional configuration of ITO/PEDOT:PSS/polymer/$PC_{71}BM$/Ca/Al, the ITO substrates were cleaned and exposed to a 30 min UV/$O_3$ treatment, and then PEDOT:PSS (2000 rpm for 30 min) was spin-coated and annealed 150 $^oC$ for 15 min. After cooling to room temperature, the chlorobenzene solution of polymer/$PC_{71}BM$ mixture was spin-coated at a speed of 1000 rpm for 30 s. Then Calcium (20 nm) and aluminum (80 nm) was successively thermally evaporated on photoactive layer. The current-voltage (*J-V*) characteristics of the devices were measured by using a Keithley 2400 Source Measure Unit. The measurements were conducted under the irradiation of AM 1.5 G, 100 mW cm$^{-2}$. The external quantum efficiency (EQE) was measured by a Solar Cell Spectral Response Measurement System QE-R3011.

## Acknowledgements

This work was supported by the National Natural Science Foundation of China (Nos. 21073200, 91222203, 21273251, 21373239, 91333111, 21190034, 21221002), project of Construction of Innovative Teams and Teacher Career Development for Universities and Colleges Under Beijing Municipality (IDHT20140512), the National Basic Research Program of China (973) 2011CB808402, 2013CB933500, and the Chinese Academy of Sciences. We thank the Beijing Synchrotron Radiation Facility (beamline 1W1A) for providing the beam time.

## Notes and references

1 Y. J. Cheng, S. H. Yang and C. S. Hsu, *Chem. Rev.*, 2009, **109**, 5868-5923.
2 Y. Huang, E. J. Kramer, A. J. Heeger and G. C. Bazan, *Chem. Rev.*, 2014, **114**, 7006-7043.
3 L. Lu, T. Xu, W. Chen, E. S. Landry and L. Yu, *Nat. Photon.*, 2014, **8**, 716-722.
4 Z. He, C. Zhong, S. Su, M. Xu, H. Wu and Y. Cao, *Nat. Photon.*, 2012, **6**, 591-595.
5 Y. Wang, X. Xin, Y. Lu, T. Xiao, X. Xu, N. Zhao, X. Hu, B. S. Ong and S. C. Ng, *Macromolecules*, 2013, **49**, 9587-9592.
6 C. Liu, W. Cai, X. Guan, C. Duan, Q. Xue, L. Ying, F. Huang and Y. Cao, *Polym. Chem.*, 2013, **4**, 3949-3958.
7 J. Zhou, S. Xie, E. F. Amond and M. L. Becker, *Macromolecules*, 2013, **46**, 3391-3394.
8 G. Li, R. Zhu and Y. Yang, *Nat. Photon.*, 2012, **6**, 153-161.
9 J. Gao, W. Chen, L. Dou, C.-C. Chen, W.-H. Chang, Y. Liu, G. Li and Y. Yang, *Adv. Mater.*, 2014, **26**, 3142-3147.
10 J. E. Coughlin, Z. B. Henson, G. C. Welch and G. C. Bazan, *Acc. Chem. Res.*, 2013, **47**, 257-270.
11 L. Pandey, C. Risko, J. E. Norton and J.-L. Brédas, *Macromolecules*, 2012, **45**, 6405-6414.
12 M. Helgesen, R. Sondergaard and F. C. Krebs, *J. Mater. Chem.*, 2010, **20**, 36-60.
13 J. Lee, A. R. Han, H. Yu, T. J. Shin, C. Yang and J. H. Oh, *J. Am. Chem. Soc.*, 2013, **135**, 9540-9547.
14 P. Sonar, S. P. Singh, Y. Li, M. S. Soh and A. Dodabalapur, *Adv. Mater.*, 2010, **22**, 5409-5413.
15 I. Kang, H.-J. Yun, D. S. Chung, S.-K. Kwon and Y.-H. Kim, *J. Am. Chem. Soc.*, 2013, **135**, 14896-14899.
16 R. S. Ashraf, I. Meager, M. Nikolka, M. Kirkus, M. Planells, B. C. Schroeder, S. Holliday, M. Hurhangee, C. B. Nielsen, H. Sirringhaus and I. McCulloch, *J. Am. Chem. Soc.*, 2014, **137**, 1314-1321.
17 H. Bronstein, Z. Chen, R. S. Ashraf, W. Zhang, J. Du, J. R. Durrant, P. Shakya Tuladhar, K. Song, S. E. Watkins, Y. Geerts, M. M. Wienk, R. A. J. Janssen, T. Anthopoulos, H. Sirringhaus, M. Heeney and I. McCulloch, *J. Am. Chem. Soc.*, 2011, **133**, 3272-3275.
18 W. Li, K. H. Hendriks, A. Furlan, W. S. C. Roelofs, S. C. J. Meskers, M. M. Wienk and R. A. J. Janssen, *Adv. Mater.*, 2014, **26**, 1565-1570.
19 K. H. Hendriks, G. H. L. Heintges, V. S. Gevaerts, M. M. Wienk and R. A. J. Janssen, *Ang. Chem. Int. Ed.*, 2013, **52**, 8341-8344
20 A. T. Yiu, P. M. Beaujuge, O. P. Lee, C. H. Woo, M. F. Toney and J. M. J. Fréchet, *J. Am. Chem. Soc.*, 2012, **134**, 2180-2185.

21 B. Fu, J. Baltazar, A. R. Sankar, P.-H. Chu, S. Zhang, D. M. Collard and E. Reichmanis, *Adv. Funct. Mater.*, 2014, **24**, 3734-3744.
22 M. Kirkus, L. Wang, S. Mothy, D. Beljonne, J. Cornil, R. A. Janssen and S. C. Meskers, *J. Phys. Chem. A*, 2012, **116**, 7927-7936.
23 R. Rieger, D. Beckmann, A. Mavrinskiy, M. Kastler and K. Müllen, *Chem. Mater.*, 2010, **22**, 5314-5318.
24 Y. Wu, Z. Li, W. Ma, Y. Huang, L. Huo, X. Guo, M. Zhang, H. Ade and J. Hou, *Adv. Mater.*, 2013, **25**, 3449-3455.
25 T. Lei, Y. Cao, X. Zhou, Y. Peng, J. Bian and J. Pei, *Chem. Mater.*, 2012, **24**, 1762-1770.
26 W. Lee, G.-H. Kim, S.-J. Ko, S. Yum, S. Hwang, S. Cho, Y.-H. Shin, J. Y. Kim and H. Y. Woo, *Macromolecules*, 2014, **47**, 1604-1612.
27 T. L. Nguyen, H. Choi, S.-J. Ko, M. A. Uddin, B. Walker, S. Yum, J.-E. Jeong, M. H. Yun, T. Shin, S. Hwang, J. Y. Kim and H. Y. Woo, *Energy Environ. Sci.*, 2014, **7**, 3040-3051.
28 H. Bürckstümmer, A. Weissenstein, D. Bialas and F. Würthner, *J. Org. Chem.*, 2011, **76**, 2426-2432.
29 R. Qin, W. Li, C. Li, C. Du, C. Veit, H.-F. Schleiermacher, M. Andersson, Z. Bo, Z. Liu, O. Inganäs, U. Wuerfel and F. Zhang, *J. Am. Chem. Soc.*, 2009, **131**, 14612-14613.
30 E. Zhou, S. Yamakawa, Y. Zhang, K. Tajima, C. Yang and K. Hashimoto, *J. Mater. Chem.*, 2009, **19**, 7730.
31 J.-Y. Wang, S. K. Hau, H.-L. Yip, J. A. Davies, K.-S. Chen, Y. Zhang, Y. Sun and A. K. Y. Jen, *Chem. Mater.*, 2011, **23**, 765-767.
32 T. Lei, Y. Cao, Y. Fan, C.-J. Liu, S.-C. Yuan and J. Pei, *J. Am. Chem. Soc.*, 2011, **133**, 6099-6101.
33 D. H. Lee, J. Shin, M. J. Cho and D. H. Choi, *Chem. Commun.*, 2013, **49**, 3896-3898.
34 T. I. Ryu, Y. Yoon, J.-H. Kim, D.-H. Hwang, M. J. Ko, D.-K. Lee, J. Y. Kim, H. Kim, N.-G. Park, B. Kim and H. J. Son, *Macromolecules*, 2014, **47**, 6270-6280.
35 C. J. Brabec, A. Cravino, D. Meissner, N. S. Sariciftci, T. Fromherz, M. T. Rispens, L. Sanchez and J. C. Hummelen, *Adv. Funct. Mater.*, 2001, **11**, 374-380.
36 D. Mori, H. Benten, I. Okada, H. Ohkita and S. Ito, *Energy Environ Sci.*, 2014, **7**, 2939-2943.
37 N. C. Cates, R. Gysel, Z. Beiley, C. E. Miller, M. F. Toney, M. Heeney, I. McCulloch and M. D. McGehee, *Nano Lett.*, 2009, **9**, 4153-4157.
38 W. Li, K. H. Hendriks, A. Furlan, W. S. C. Roelofs, M. M. Wienk and R. A. J. Janssen, *J. Am. Chem. Soc.*, 2013, **135**, 18942-18948.

for Table of Content only

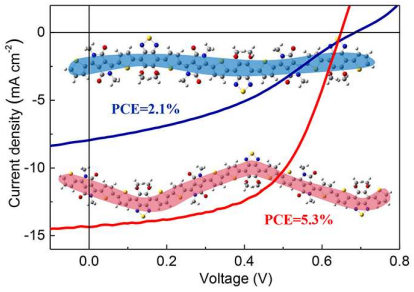


Two polymer semiconductors with different degree of chain curvature are designed and synthesized. The curved polymer blended with $PC_{71}BM$ exhibits higher PCE of 5.3% than that of linear polymer.